Realistic Stripline Corner Modeling Using Surrogate Model and Topographic Fitting

[1]Andrew Page, [1]Matteo Cocchini, [1]Zhaoqing Chen, [2]Xu Chen
[1]*IBM Systems, Poughkeepsie, NY 12601, USA*
[2]*Department of Electrical and Computer Engineering, University of Illinois Urbana–Champaign, Urbana, IL 61820, USA*
ajpage2@illinois.edu, mcocchi@us.ibm.com, zhaoqing@us.ibm.com, xuchen1@illinois.edu

2022 IEEE 31st Conference on Electrical Performance of Electronic Packaging and Systems (EPEPS) | 978-1-6654-5075-1/22/$31.00 ©2022 IEEE | DOI: 10.1109/EPEPS53828.2022.9947141

***Abstract*—This paper demonstrates a method to extract impedance-attenuation corners of a stripline with user-prescribed confidence levels. This is done using a sparse-grid-based surrogate model to quickly generate vast Monte Carlo datasets from which the impedance-attenuation distribution is calculated. Ellipses are fit to this distribution as equi-density contours to enclose a proportion of the solution data. Appropriate corners can be read off these ellipses and applied to broadband simulation. The results are compared against three measured test coupons, showing capability to analyze a PCIe Gen. 5 link. Realistic modeling of geometries and material variations is emphasized.**

***Index Terms*—corner model, sparse grid, Monte Carlo**

I. Introduction

Electrical interconnect performance is becoming increasingly difficult to characterize and control as the demand for fast data rates grows. Imperfect manufacturing processes lead manifested designs to not possess their intended physical properties and provide uncontrollable variation in performance characteristics. Interconnect characterization based on the nominal design is thus unrealistic. The worst-case behavior can be studied but represents a performance outlier. Corner modeling is a way to capture realistic variation from the nominal behavior. Current corner modeling algorithms rely on fast but unreliable boundary scan methods or expensive Monte Carlo (MC) procedures [1], [2].

The method proposed by this paper combines the best of both approaches by creating a surrogate model that accurately and efficiently maps cross-section and material parameters to corresponding attenuation and impedance (α, Z_0) values. This model is used to generate vast amounts of MC data, which is then binned into a 2D density. Ellipses centered on the nominal solution are fit as effective equi-density contours using an iterative algorithm. The high/low impedance/attenuation (HZLA, LZLA, HZHA, LZHA) corners can be read from the contour, and the corresponding parameter configurations can be found easily. They are then inputted to Ansys 2D Extractor for broadband S-parameter extraction and eye diagram simulation.

Section II introduces the EM simulation methodology, the surrogate model development, the contour fitting and the corner identification algorithm. Section III discusses the results of the procedure and the eye characteristics of each calculated corner, with concluding remarks offered in Section IV.

This material is based upon work supported by the National Science Foundation under Grant No. CNS 16-24811 - Center for Advanced Electronics through Machine Learning (CAEML) and its industry members.

II. The Corner Modeling Process

A. EM Simluation & Parameter Variation

The corner location procedure will be done using both a single-ended and a differential stripline, defined in Table I and Fig. 1. These models are solved with Ansys 2D Extractor at a single frequency to extract the RLGC parameters. The single-ended line's attenuation α and characteristic impedance Z_0 can be calculated at solution frequency $f = 20$GHz via

$$\alpha = \mathrm{Re}\left[(R + j\omega L)(G + j\omega C)\right], \tag{1}$$

$$Z_0 = \mathrm{Re}\left[(R + j\omega L)/(G + j\omega C)\right], \tag{2}$$

where $\omega = 2\pi f$. The differential impedance for the two-line structure is found by extracting RLGC for the left half of Fig. 1(b) and doubling the calculated impedance from (2). The attenuation is found directly from (1). Placing a conducting boundary as shown rejects all common-mode fields.

The 2D models are built to reflect consequences of realistic manufacturing procedures, including a trapezoidal conductor with angle ϕ to model chemical etching effects and holding pitch $s + w$ constant due to tight photolithography tolerances. The dielectric constant ϵ_r and tangent delta $\tan\delta$ were measured at 20GHz using short pulse propagation (SPP) [3].

A parameter ξ with a symmetric tolerance $\xi = \mu \pm 3\sigma$ is modeled as a Gaussian random variable with mean μ and standard deviation σ, i.e. a parameter's tolerance represents its

TABLE I
Parameters & Tolerances

Name	Symbol	Nominal	Tolerance	Unit
Perm.	ϵ_r	3.25	+0.25/-0.15	-
Loss Tan.	$\tan\delta$	0.00325	+0.0024/-0.0020	-
Thickness	t	0.6	+/-0.1	mil
Width	w	4.7	+/-0.6	mil
Prepreg size	h_1	4.2	+/-1.0	mil
Core size	h_2	4.0	+/-0.7	mil
Pitch	$s + w$	9	-*	mil
Gnd. width	w_{gnd}	200	-	mil
Gnd. thick.	t_{gnd}	1.2	-	mil
Edge angle	ϕ	78.23	-	deg
Cu resist.	ρ	1.9	-	$\mu\Omega$-cm

*A dashed tolerance represents a fixed parameter.

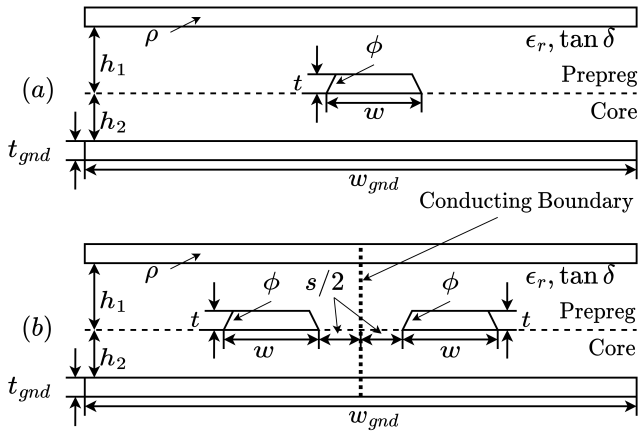

Fig. 1. Cross section of single-ended (a) and differential-mode (b) striplines. Conducting boundary can be used for efficient differential-mode impedance extraction.

3σ value. Asymmetric parameters, e.g. $\xi = \mu + 3\sigma_2/-3\sigma_1$, are modeled with a modified Gaussian distribution, characterized by probability density function with a spread of σ_1 below and σ_2 above the center value μ:

$$f(u) = \frac{2}{(\sigma_1+\sigma_2)\sqrt{2\pi}} \begin{cases} \exp\left(-\frac{(u-\mu)^2}{2\sigma_1^2}\right), & u \le \mu, \\ \exp\left(-\frac{(u-\mu)^2}{2\sigma_2^2}\right), & u > \mu. \end{cases} \quad (3)$$

B. Sparse Grid Surrogate Model

Surrogate modeling provides a way around the computational expense of MC simulation. The Tasmanian software package allows creation of such a model based on sparse grid collocation [4]. The sparse grid is a set of points in the design space that serves as a high-dimensional interpolation grid. Simulations can be run for each point in the grid, and the results can be interpolated. This interpolation can be evaluated in a split-second, and yields a good approximation to the 2D simulation of the same input. Details can be found in [5].

Interpolations for α and Z_0 at 20GHz are formed by simulating RLGC for each point on the sparse grid with 2D Extractor and interpolating the calculated (α,Z_0) over the sparse grid. Several surrogate models were tested against 4,000 MC datapoints, which each model computed in less than 110ms with mean errors less than 1% and 0.1% in α and Z_0, respectively, demonstrating the sparse grid's reliability. The selected model used a precision 3 'level' grid based on the Clenshaw-Curtis rule, taking 389 simulations to form, which is a one-time cost similar to a boundary scan [1].

C. Fitting the Equi-Density Contour

Locating the corners begins by first finding the distribution of (α, Z_0) based on parameter values from Table I. This is done with a massive MC batch to be run with the surrogate model. This paper uses two million samples, a job that would take 2D Extractor days to calculate but the surrogate model can perform in seconds. The distribution can be approximated by binning the (α, Z_0) scatter data into $n_x \times n_y = 200 \times 200$ cells and counting the number of solutions lying within each cell. The resulting density histogram resembles a hill peaking near the nominal solution. The shape and orientation of the distribution is due to the near-Gaussian input parameters and the slight nonlinear dependence of (α, Z_0) on the input parameters. This histogram can be characterized by equi-density contours, as in a topographical map. The histogram's shape suggests the ellipse as a good equi-density contour.

Three coordinate systems are defined to help identify the ellipse: (α, Z_0) is the main working system, (x, y) results from centering and normalizing (α, Z_0), and (η, ν) is a version of (x, y) rotated by θ_f so the η axis aligns with the semimajor axis of the ellipse, as summarized in (4) and (5). Attenuation and impedance ranges are denoted $\Delta\alpha$ and ΔZ_0.

$$R = \begin{pmatrix} \cos\theta_f & -\sin\theta_f \\ \sin\theta_f & \cos\theta_f \end{pmatrix}, \quad M = \begin{pmatrix} \Delta\alpha/n_x & 0 \\ 0 & \Delta Z_0/n_y \end{pmatrix}, \quad (4)$$

$$\begin{pmatrix} \alpha \\ Z_0 \end{pmatrix} = \begin{pmatrix} \alpha_{nom} \\ Z_{0,nom} \end{pmatrix} + M \begin{pmatrix} x \\ y \end{pmatrix}, \quad \begin{pmatrix} x \\ y \end{pmatrix} = R \begin{pmatrix} \eta \\ \nu \end{pmatrix}. \quad (5)$$

The ellipse will lie in (α, Z_0) space centered on the nominal solution $(\alpha_{nom}, Z_{0,nom})$. Its orientation can be found by first specifying a threshold percentage of the peak density, like an equipotential contour on a topographical map. A sweep of the angle from the x-axis, θ, tracking the distance r to the prescribed threshold in (x, y)-space is fit into (6). The tilt angle θ_f and semimajor/minor axes a and b thus can be recovered.

$$r^2(\theta) = \left(\frac{\cos^2(\theta - \theta_f)}{a^2} + \frac{\sin^2(\theta - \theta_f)}{b^2} \right)^{-1}. \quad (6)$$

This procedure is iterated by lowering the threshold until the ellipse encloses a certain proportion of the solution data, i.e. a given inclusion rate. A solution's inclusion within the contour can be tested by evaluating the face equation of (7) after appropriate transformation to (η, ν) using (4) and (5):

$$\text{contour:} \quad \frac{\eta^2}{a^2} + \frac{\nu^2}{b^2} = 1; \quad \text{face:} \quad \frac{\eta^2}{a^2} + \frac{\nu^2}{b^2} \le 1. \quad (7)$$

D. Corner Identification

The corners can be read off this ellipse through any desired means. This paper employs a procedure based on [1]. The ellipse can be bound by a rectangle sharing its extreme α and Z_0 values, i.e. $\alpha = \alpha_{nom} \pm \delta\alpha$, $Z_0 = Z_{0,nom} \pm \delta Z_0$. The impedance is then scaled by $C = \delta\alpha/\delta Z_0$ after shifting to the origin, which stretches the rectangle into a square of length $2\delta\alpha$ and scales the ellipse impedance extrema to $\pm\delta\alpha$. The corners are read as each intersection of the ellipse and the diagonals of the square, reverting to (α, Z_0) using the scaling.

III. Numerical Examples

The procedure outlined in Section II was applied to single-ended and differential models with 1σ, 2σ and 3σ inclusions (68%, 95% and 99%). The corners were located using the scaling method, as shown in Fig. 2 for the 3σ differential case. The three differential-line ellipses are shown with the

MC scatter data in Fig. 3. Table II lists the parameters for each 3σ corner, each behaving as expected; low-Z corners share high widths, low-A corners share low loss tangents.

Three test coupons were measured for model validation. The (α, Z_0) of each coupon was found using VNA measurements and simulated TDR, and are plotted in Fig. 3. Each fall within the 2σ contour, demonstrating the inclusion as a confidence in the performance of a manufactured board. The four 3σ corners were run in a broadband simulation to compute their S-parameters as 7cm lines. The dielectric was modeled with a multipole Debye fit based on measured data [6]. The insertion losses of each model, summarized in Table III, are compared at the fundamental frequencies of PCIe Gen. 4 and 5 (8 and 16GHz, respectively), and the material characterization frequency of 20GHz. The corners form a bound on the insertion loss, bounded below by HZLA and above by LZHA.

The eye was simulated using a PRBS-23 sequence with a rate of 32Gbps and a 7ps rise/fall time, to emulate the line as a PCIe Gen. 5 link. The results are summarized in Table IV. The high-A corners showed the smallest eye heights. The eye width sensitivity is accentuated by the line length, showing low sensitivity in general. A similar bounding on the eye characteristics based on the inclusion level is expected.

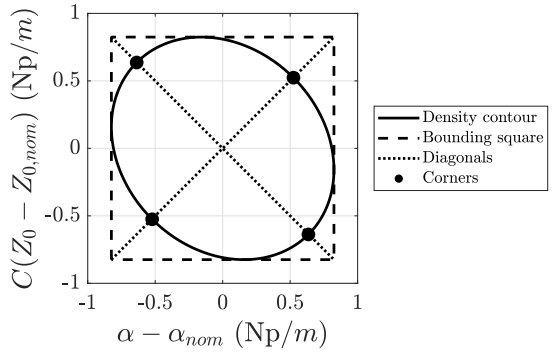

Fig. 2. Differential-line 3σ-inclusion ellipse and bounding square in scaled/centered attenuation-impedance space.

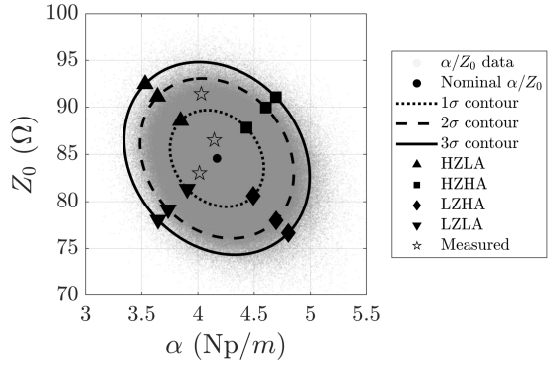

Fig. 3. Samples of differential-line MC data with derived equi-density contours and corners for 1σ, 2σ and 3σ inclusion.

IV. Conclusion

The proposed corner modeling scheme is capable of characterizing PCIe Gen. 5 interconnect performance. A well-trained surrogate model makes the process as expensive as a boundary scan. The scheme offers flexibility in the precise control of the inclusion rate. The simplicity of the contour choice allows for easy implementation while maintaining accurate results. Further work may include a more robust density-finding algorithm based on kernel density estimation.

References

[1] Z. Chen, "Transmission line attenuation-impedance realistic corner modeling by scaled-down tolerance boundary scan," in *2007 IEEE International Symposium on Electromagnetic Compatibility*, 2007, pp. 1–6.

[2] N. Lu, "Statistical and corner modeling of interconnect resistance and capacitance," in *IEEE Custom Integrated Circuits Conference 2006*, 2006, pp. 853–856.

[3] A. Deutsch, R. Krabbenhoft, K. Melde, C. Surovic, G. Katopis, G. Kopcsay, Z. Zhou, Z. Chen, Y. Kwark, T.-M. Winkel, X. Gu, and T. Standaert, "Application of the short-pulse propagation technique for broadband characterization of pcb and other interconnect technologies," *Electromagnetic Compatibility, IEEE Transactions on*, vol. 52, pp. 266 – 287, 06 2010.

[4] M. Stoyanov, D. Lebrun-Grandie, J. Burkardt, and D. Munster, "Tasmanian," 9 2013. [Online]. Available: https://github.com/ORNL/Tasmanian

[5] M. Stoyanov, "User manual: Tasmanian sparse grids," Oak Ridge National Laboratory, One Bethel Valley Road, Oak Ridge, TN, Tech. Rep. ORNL/TM-2015/596, 2015.

[6] A. E. Engin, I. Ndip, K.-D. Lang, and J. Aguirre, "Closed-form multipole debye model for time-domain modeling of lossy dielectrics," *IEEE Transactions on Electromagnetic Compatibility*, vol. 61, no. 3, pp. 966–968, 2019.

TABLE II
3σ Corner Parameter Configurations

Param.	ϵ_r	$\tan\delta$	t	w	h_1	h_2
Unit	-	-	mil	mil	mil	mil
	Differential (fixed 9mil pitch)					
HZLA	3.25	0.00170	0.607	4.47	5.25	4.15
LZLA	3.23	0.00159	0.689	4.98	3.79	4.13
HZHA	3.22	0.00503	0.591	4.42	4.45	4.24
LZHA	3.26	0.00449	0.605	4.82	3.29	4.07
	Single-Ended					
HZLA	3.12	0.00190	0.633	4.43	4.66	4.20
LZLA	3.34	0.00155	0.576	5.11	3.80	4.20
HZHA	3.43	0.00472	0.650	4.43	4.78	4.56
LZHA	3.23	0.00461	0.646	4.80	3.36	4.10

TABLE III
Insertion Loss Comparison Against Measurement

	Insertion loss (dB)						
f	3σ Corners				Measured		
(GHz)	HZLA	LZLA	HZHA	LZHA	#1	#2	#3
8	1.15	1.42	1.36	1.67	1.31	1.30	1.26
16	1.82	2.20	2.21	2.69	2.13	2.08	2.06
20	2.14	2.42	2.65	3.02	2.52	2.44	2.45

TABLE IV
Eye Characteristics of 7cm & 20cm Line

	7cm line		20cm line	
	Height (mV)	Width (UI)	Height (mV)	Width (UI)
Nominal	379.34	0.9202	247.58	0.7545
HZLA	385.15	0.9261	260.61	0.7725
LZLA	368.73	0.9202	242.02	0.7345
HZHA	347.85	0.8603	213.38	0.7345
LZHA	355.33	0.9022	180.10	0.6826